JOURNAL OF GUIDANCE, CONTROL, AND DYNAMICS
Vol. 38, No. 9, September 2015

Formation Establishment and Reconfiguration Using Differential Elements in *J2*-Perturbed Orbits

Christopher W. T. Roscoe,* Jason J. Westphal,† and Jacob D. Griesbach‡
Applied Defense Solutions, Columbia, Maryland 21044
and
Hanspeter Schaub§
University of Colorado, Boulder, Colorado 80309

DOI: 10.2514/1.G000999

A computationally efficient algorithm is developed for onboard planning of n-impulse fuel-optimal maneuvers for establishment and reconfiguration of spacecraft formations. The method is valid in circular and elliptic orbits and includes first-order secular J_2 effects. The dynamics are expressed in terms of differential mean orbital elements, and relations are provided to allow the formation designer to transform these into intuitive geometric quantities for visualization and analysis. The maneuver targeting problem is formulated as an optimal control problem in both continuous and discrete time. The continuous-time formulation cannot be solved directly in an efficient manner, and the discrete-time formulation, which has an analytical solution, does not directly yield the optimal thrust times. Therefore, a new flight-suitable algorithm is designed by iteratively solving the discrete-time formulation while using the continuous-time necessary conditions to refine the thrust times until they converge to the optimal values. Simulation results illustrate the performance for a variety of reconfiguration maneuvers and reference orbits, including examples for the NASA CubeSat Proximity Operations Demonstration mission.

I. Introduction

SPACECRAFT formation flying is a key area of research in modern spacecraft dynamics and control. Numerous formation flying missions have been conceived over the past two decades and many have flown successfully. This concept enables several mission types including sparse apertures, where multiple spacecraft take the place of a large antenna or telescope, magnetic and electrical interaction studies, and on-orbit servicing or inspection. One important area of research in this field is the development of algorithms for establishing or reconfiguring a formation. The present work is motivated by the upcoming NASA CubeSat Proximity Operations Demonstration (CPOD) mission. CPOD, sponsored by the NASA Office of the Chief Technologist, is to demonstrate formation flying and docking of a pair of three-unit CubeSats using miniaturized navigation and propulsion. The algorithm defined in this paper is to form the basis of the CPOD guidance system for onboard maneuver planning.

Formation establishment or reconfiguration is defined as the process of taking a spacecraft formation from some initial configuration and transforming it to another configuration. This is necessary to, for example, establish a synthetic aperture, initiate or change proximity operations trajectories for inspection of a debris object, or recover from a period of uncontrolled drift. The main problem addressed in this paper is that of designing maneuvers, made up of n impulsive thrusts, to take a spacecraft formation from some initial trajectory to a desired trajectory with as little fuel as possible.

This is by no means a new problem and it has been investigated by numerous authors in the past. However, the previous methods suffer from one or more of the following drawbacks:

1) They involve the computationally expensive and sensitive solution of sets of nonlinear equations [1–13].
2) They assume a circular or near-circular reference orbit [1–4,6,9,10,13–16].
3) They assume a set of impulse times and do not solve for the optimal ones [15–22].
4) They minimize fuel use for each thrust axis independently [14,17,18].

Some of these issues may not be critical for certain specific mission profiles, but the goal of this paper is to design a general method for optimal maneuver targeting in circular or elliptic reference orbits, including the J_2 perturbation, which can be implemented onboard a spacecraft with limited computational power.

This goal is accomplished by using an approach similar to Lawden's primer vector theory [23], as in [1–8,10,11]. However, instead of solving the nonlinear equations directly, a suboptimal, discrete-time formulation is iteratively refined, using the necessary conditions of the continuous-time system to find the optimal impulse times. The discrete formulation is analytically solvable with the use of differential orbital elements as state variables. Similar discrete solvable formulations have been used by Breger and How [17], Roth [20], Saunders [16], Anderson and Schaub [21], and Gaias et al. [22], where the problem is broken up into many segments and the overall fuel cost is minimized, but these methods typically allow more impulses than necessary and do not find the true optimal times.

Of the previous work, only Gaias et al. [22] include differential drag in the analytical model, which is a primary consideration in low Earth orbit. However, it is challenging to model this perturbation accurately for general spacecraft formations because of its dependence on the attitude and shape of both spacecraft and because of problems with modeling atmospheric density and surface interactions. It is possible, given accurate knowledge of on-orbit attitude profiles, to estimate the differential ballistic coefficient of the spacecraft to aid the onboard maneuver planning process (e.g., as is the case in the PRISMA navigation system [24]). However, in some cases, attempting to simulate drag effects with uncertain attitude and density knowledge can result in less accurate state propagation than if drag were not included in the force model at all [25]. Therefore, the present work does not address this perturbation, which implicitly invokes the assumption that either the ballistic coefficients of the

Received 22 August 2014; revision received 12 April 2015; accepted for publication 22 May 2015; published online 23 July 2015.

*Aerospace Engineer; CRoscoe@applieddefense.com. Member AIAA.
†Senior Aerospace Engineer; JWestphal@applieddefense.com. Member AIAA.
‡Technical Director; JGriesbach@applieddefense.com.
§Professor, Associate Chair of Undergraduate Affairs, Department of Aerospace Engineering Sciences; hanspeter.schaub@colorado.edu. Associate Member AIAA.

spacecraft in the formation are very similar or the orbit altitude is high enough that differential drag effects are small.

The dynamic equations in this paper are developed in terms of mean orbital element differences rather than Cartesian coordinates. Differential orbital elements are a natural and convenient choice for designing general formations [26,27] because they provide several mathematical advantages over Cartesian coordinates for describing relative motion: They vary slowly, because they are constants of the unperturbed motion, and using mean elements allows for the explicit inclusion of secular J_2 effects. Furthermore, using a set of nearly nonsingular elements makes the solution uniformly applicable to both circular and elliptic orbits. Finally, although they provide only indirect insight into the shape, size, and location of the relative orbit, they can be readily transformed into mission-useful quantities, such as size, orientation, etc., for visualization and analysis [28,29]. Differential elements (in the form of relative eccentricity/inclination vectors [30]) have been successfully used for guidance and control of the PRISMA [31] and TanDEM-X/TerraSAR-X [32] missions. In the ARGON experiment, conducted during the extended phase of the PRISMA mission, navigation was also performed by directly estimating the relative eccentricity/inclination vectors, rather than computing them from relative position and velocity [33].

From the overall system design standpoint, the best approach to solving the problem is to use the most efficient mathematical form (differential mean orbital elements) to describe the dynamics but allow the formation designer to interact with more intuitive geometric quantities. The maneuver targeting problem is formulated as an optimal control problem in which the analytical solution to the unforced dynamics is given by the Gim–Alfriend state transition matrix (STM) [34] and the control influence is given by Gauss's variational equations (GVEs) [35], reformulated in terms of the nearly nonsingular elements. Similar approaches have been used by previous authors to solve feedback control problems using classical mean orbital elements [17,18,36–39]. The formation designer can then apply this method by defining a desired formation in terms of size and orientation parameters and then converting to differential elements for maneuver targeting.

The paper is laid out as follows. In Sec. II, the formation dynamics are defined in terms of differential nearly nonsingular mean orbital elements. In Sec. III, the minimum-fuel maneuver targeting problem is defined, and the necessary conditions for optimality are derived. Section IV discusses a computationally efficient algorithm for onboard maneuver targeting, in which the discrete-time problem is iteratively solved while using the continuous-time necessary conditions to refine the thrust times until they converge to the optimal values. Finally, Sec. V provides simulation results for a variety of reconfiguration maneuvers and reference orbits. This includes simulations for the CPOD mission, as well as a comparison to the impulsive maneuver targeting method of Anderson and Schaub [21].

II. Formation Dynamics

A general spacecraft formation consists of two or more space objects flying in close proximity to one another. The term "close" is defined such that the relative motion between the objects can be linearized about some reference orbit (this depends on the orbit of the formation and the required accuracy of the motion). Spacecraft in the formation can act either cooperatively or noncooperatively and the reference orbit need not correspond to an actual physical object. Without loss of generality, in this paper, the formation is assumed to consist of only two spacecraft. One spacecraft, which defines the reference orbit, is designated the "chief," and it is uncontrolled. The other spacecraft is designated the "deputy," and it is controlled by a three-component thrust input.

The dynamics of relative motion are defined in terms of differential orbital elements, but formation configurations and visualizations are presented in Cartesian coordinates as well, using the local-vertical/local-horizontal (LVLH) reference frame. This frame, shown in Fig. 1, is defined with $\hat{\boldsymbol{h}}_r$ in the radial direction, $\hat{\boldsymbol{h}}_h$ in the orbit normal direction, and $\hat{\boldsymbol{h}}_t$ completing the right-hand system. The mapping

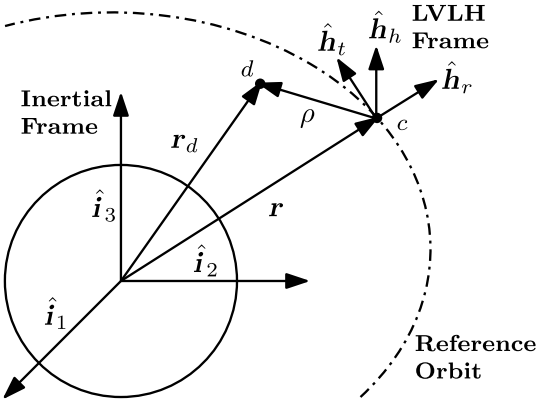

Fig. 1 LVLH reference frame.

between differential orbital elements and LVLH coordinates can be found in a number of references (e.g., [28,34,40]).

A. Formation Dynamics in Nearly Nonsingular Mean Orbital Elements

The nearly nonsingular mean orbital elements of the reference (chief) orbit are defined as

$$\text{œ} = [\,a \quad \lambda \quad i \quad q_1 \quad q_2 \quad \Omega\,]^T \tag{1}$$

where a is the semimajor axis, $\lambda = M + \omega$ is the mean argument of latitude, M is the mean anomaly, ω is the argument of perigee, i is the inclination, $q_1 = e\cos\omega$ and $q_2 = e\sin\omega$ are the orbital frame components of the eccentricity vector, e is the eccentricity, and Ω is the right ascension of the ascending node. This set of orbital elements is chosen instead of the classical orbital elements because it is not singular in the case of a circular orbit; however, it is still singular in an equatorial orbit. This set of coordinates is very suitable for low-Earth-orbit operations where equatorial orbits are vanishingly rare. Compared with fully nonsingular elements, such as the equinoctial elements, the associated mathematical formulations are greatly simplified.

The transformation from the osculating elements œ′ to the mean elements is defined by

$$\text{œ} = \boldsymbol{g}(\text{œ}') \tag{2}$$

The full transformation is given by Brouwer's analytical satellite theory [41], and a first-order truncation is given by Schaub and Junkins [42, Appendix F]. Including the effects of J_2, the mean elements evolve according to

$$\dot{\text{œ}} = \boldsymbol{f}(\text{œ}) + \boldsymbol{g}(B(\text{œ}')\boldsymbol{u}) \tag{3}$$

The unforced dynamics are given by a modified form of Lagrange's planetary equations (LPEs) for J_2 [35],

$$\boldsymbol{f}(\text{œ}) = \begin{bmatrix} 0 \\ n + \frac{3}{4}J_2\left(\frac{R_e}{p}\right)^2 n[\eta(3\cos^2 i - 1) + (5\cos^2 i - 1)] \\ 0 \\ -\frac{3}{4}J_2\left(\frac{R_e}{p}\right)^2 n(3\cos^2 i - 1)q_2 \\ \frac{3}{4}J_2\left(\frac{R_e}{p}\right)^2 n(3\cos^2 i - 1)q_1 \\ -\frac{3}{2}J_2\left(\frac{R_e}{p}\right)^2 n\cos i \end{bmatrix} \tag{4}$$

where J_2 is the coefficient of the second zonal harmonic, R_e is the mean equatorial radius of the Earth, p is the semilatus rectum, n is the mean motion, and $\eta = \sqrt{1 - e^2}$.

The vector $\boldsymbol{u}$ is a thrust input defined in the LVLH frame

$$\boldsymbol{u} = [\, u_r \quad u_t \quad u_h \,]^T \tag{5}$$

whose effect on the osculating orbital elements is given by a modified form (to use the nearly nonsingular elements) of GVEs $B(\text{œ}')$, given in Appendix A. Because GVEs give the effect of accelerations on the osculating elements, the osculating–mean transformation must then be applied to determine changes in the mean elements. However, the sensitivities of mean element changes with respect to osculating element changes are of at most $\mathcal{O}(J_2)$; therefore, for small accelerations, it is reasonable to approximate Eq. (3) with [36,37]

$$\dot{\text{œ}} \approx \boldsymbol{f}(\text{œ}) + B(\text{œ})\boldsymbol{u} \tag{6}$$

The motion of the deputy about the reference orbit is described by a set of differential mean orbital elements, which are related to the deputy's mean elements by

$$\delta\text{œ} = \text{œ}_d - \text{œ} \tag{7}$$

Assuming the differences between the deputy's mean elements and the reference elements are small, the dynamics of the differential mean elements are found by linearizing Eq. (6) about the reference orbit:

$$\delta\dot{\text{œ}} = A\delta\text{œ} + B\boldsymbol{u} \tag{8}$$

where B represents the GVE evaluated on the reference orbit and

$$A = \left.\frac{\partial \boldsymbol{f}}{\partial \text{œ}}\right|_{\text{œ}} \tag{9}$$

is the Jacobian of the LPE evaluated on the reference orbit. The definition of A is found in Appendix B.

B. State Transition Matrix for Differential Elements

The general solution to Eq. (8) is given by

$$\delta\text{œ}(t) = \boldsymbol{\Phi}(t, t_0)\delta\text{œ}(t_0) + \int_{t_0}^{t} \boldsymbol{\Phi}(t, \tau)B(\tau)\boldsymbol{u}(\tau)\,\mathrm{d}\tau \tag{10}$$

where $\boldsymbol{\Phi}(t_2, t_1)$ is the STM of A from t_1 to t_2. The STM for the differential nearly nonsingular mean orbital elements is derived by Gim and Alfriend [34]. The STM found in that paper requires a small modification because it uses the true argument of latitude $\theta = f + \omega$ instead of the mean argument of latitude λ. For formations in near-circular reference orbits, significant computation effort is saved by using the small-eccentricity version of the STM given by Alfriend and Yan [43].

C. Initial Differential Elements for General Formations

For the trajectory designer to make use of the dynamic formulation in terms of differential orbital elements, relationships can be defined to convert formation size and orientation parameters into nearly nonsingular element differences. Sengupta and Vadali [29] define one such set of parameters, based on the general solution to the Tschauner–Hempel (TH) [44] or Lawden's [23] equations, which are summarized here for reference:

$$\delta a = \frac{-2\eta v_d}{3n} \tag{11}$$

$$\delta\lambda = \frac{\rho_2}{p} - \delta\Omega\,\cos\,i - \frac{1+\eta+\eta^2}{1+\eta}\frac{\rho_1}{p}(q_1\,\cos\,\tilde{\alpha}_0 - q_2\,\sin\,\tilde{\alpha}_0) \tag{12}$$

$$\delta i = \frac{\rho_3}{p}\cos\tilde{\beta}_0 \tag{13}$$

$$\delta q_1 = -(1-q_1^2)\frac{\rho_1}{p}\sin\,\tilde{\alpha}_0 + q_1 q_2\frac{\rho_1}{p}\cos\,\tilde{\alpha}_0 - q_2\left(\frac{\rho_2}{p} - \delta\Omega\,\cos\,i\right) \tag{14}$$

$$\delta q_2 = -(1-q_2^2)\frac{\rho_1}{p}\cos\,\tilde{\alpha}_0 + q_1 q_2\frac{\rho_1}{p}\sin\,\tilde{\alpha}_0 + q_1\left(\frac{\rho_2}{p} - \delta\Omega\,\cos\,i\right) \tag{15}$$

$$\delta\Omega = \frac{-\rho_3}{p}\frac{\sin\,\tilde{\beta}_0}{\sin\,i} \tag{16}$$

where ρ_1 and ρ_3 relate to the amplitude of the in-plane and out-of-plane motion, $\tilde{\alpha}_0$ and $\tilde{\beta}_0$ are the initial phase angles (with respect to $\lambda = 0$), ρ_2 determines how far offset the motion is in the along-track direction, and v_d is the along-track drift rate. Equations (11–16) are used to specify the initial and desired formations for the reconfigurations demonstrated in Sec. V.

To more closely approximate the well-known Hill–Clohessy–Wiltshire (HCW) [45,46] trajectories for the case of an eccentric orbit, a number of corrections are possible [29]. For example, setting

$$\rho_{2a} = \frac{2\eta^2 d}{3-\eta^2} \tag{17}$$

in a leader–follower configuration modifies the along-track offset so that the time-averaged deputy–chief separation is d. Similarly, setting

$$\rho_{2b} = \rho(q_1\,\cos\,\tilde{\alpha}_0 - q_2\,\sin\,\tilde{\alpha}_0) \tag{18}$$

in an in-plane ellipse with $d = 0$ corrects the along-track bias so that $y(-\tilde{\alpha}_0) = 2\rho$ and $y(\pi - \tilde{\alpha}_0) = -2\rho$ (this is just one possible bias correction). For an in-plane ellipse with nonzero d, use $\rho_2 = \rho_{2a} + \rho_{2b}$. Both of these equations reduce to the HCW parameters for circular orbits.

III. Fuel-Optimal Targeting of n-Impulse Maneuvers

The main problem addressed in this paper is that of finding optimal minimum-fuel maneuvers, made up of n impulsive thrusts, for formation reconfiguration. In this paper, unlike some other formulations, the minimum-fuel problem is stated in terms of the two norm of the thrust input instead of one norm. In general, even if multiple thrusters are available, it saves fuel to align the net thrust direction with one of the thrusters (or pair of coaligned thrusters) when thrust is required in more than one LVLH direction, due to the triangle inequality. The fuel savings are greater for larger maneuvers because the extra fuel cost is proportional to the total cost. That is, for smaller maneuvers, it might make more sense, operationally, to spend the small amount of extra fuel to use multiple thrusters to achieve a maneuver and not disrupt the attitude of the spacecraft.

In this section, the minimum-fuel n-impulse maneuver targeting problem is stated in both continuous- and discrete-time forms and the necessary conditions for optimality are derived. Neither of these formulations adequately solves the problem on its own, but recognizing the duality of the continuous and discrete formulations under certain conditions allows a convenient solution to be found. In the section that follows, a computationally efficient algorithm for onboard maneuver targeting is described, which uses an iterative refinement of the discrete-time form of the problem to solve for the optimal thrust times and impulse magnitudes.

A. Continuous-Time Optimal Control Problem

First, the minimum-fuel problem is defined in terms of the continuous-time dynamics. The analysis is similar to a formation flying application of Lawden's primer vector [23] theory, which is

described in detail by McAdoo et al. [47] and Jezewski [48]. A number of previous authors have used primer vector theory to address the formation reconfiguration problem in terms of Cartesian states [1–8,10,11]. The difference in this formulation is that the primer vector now depends on all six orbit element costates through GVEs, which are time varying, instead of only on the three-component velocity costate as in the Cartesian case.

The fuel cost for an n-impulse maneuver is defined as

$$J = \int_0^{t_n} \gamma(t)\,\mathrm{d}t \tag{19}$$

where $\gamma(t)$ is the impulse magnitude at time t, such that

$$\gamma(t) = \gamma_1\delta(t-t_1) + \gamma_2\delta(t-t_2) + \cdots + \gamma_n\delta(t-t_n) \tag{20}$$

and the thrust is defined by

$$\boldsymbol{u} = \gamma\hat{\boldsymbol{u}} \tag{21}$$

where $\delta(t-t_i)$ is the Dirac delta function and all $\gamma_i > 0$. Note that the final impulse is constrained to occur at the final time, which is free. According to the sifting property of delta function, this cost is exactly the sum of the impulse magnitudes

$$J = \sum_{i=1}^{n} \gamma_i \tag{22}$$

which is the total ΔV of the maneuver. The control goal is to determine the optimal γ_i, t_i, and $\hat{\boldsymbol{u}}$ to take the system from a fixed initial state $\delta\text{œ}_0$ to a desired final state $\delta\text{œ}_n = \delta\text{œ}_f$ (fixed final state).

1. Necessary Conditions for Optimality

Incorporating the system dynamics defined in Eq. (8), the Hamiltonian can be written as

$$H = \gamma + \boldsymbol{\lambda}^T(A\delta\text{œ} + \gamma B\hat{\boldsymbol{u}}) \tag{23}$$

On an optimal trajectory, the costate equation is

$$\dot{\boldsymbol{\lambda}} = -H_{\delta\text{œ}} = -A^T\boldsymbol{\lambda} \tag{24}$$

and both the costate and its derivative must be continuous, where the subscript indicates partial differentiation. The solution to the costate equation is given by

$$\boldsymbol{\lambda}(t) = \boldsymbol{\Phi}^T(t_0, t)\boldsymbol{\lambda}(t_0) \tag{25}$$

(see proof in Appendix C). Because the control direction $\hat{\boldsymbol{u}}$ appears linearly in H, the optimal control cannot be determined directly from the stationary condition. Applying Pontryagin's minimum principle, the control direction that minimizes the Hamiltonian is

$$\hat{\boldsymbol{u}} = -B^T\boldsymbol{\lambda} = -\boldsymbol{p} \tag{26}$$

where $\boldsymbol{p}$ is defined as the primer vector, a formation flying analogue to Lawden's primer vector [23]. As mentioned earlier, the difference between this formulation and previous primer vector-based formation flying analyses is that $\boldsymbol{p}$ now depends on all six orbit element costates through GVEs, the time-varying B matrix, instead of only on the three-component velocity costate.

Applying the necessary condition for the control direction, the Hamiltonian then becomes

$$H = (1 - \boldsymbol{p}^T\boldsymbol{p})\gamma + \boldsymbol{\lambda}^T A\delta\text{œ} \tag{27}$$

Optimal control theory requires that both the Hamiltonian and the costate must be continuous throughout an optimal trajectory ([49] Chapter 5). Because H must be continuous, the coefficient of γ must be zero when each impulse is applied:

$$\|\boldsymbol{p}\| = p = 1, \quad \forall\ t = t_i \tag{28}$$

At other times, for the trajectory to be optimal, $p < 1$ or else Pontryagin's minimum principle would imply that the trajectory is nonoptimal because some additional nonzero γ exists, which would decrease the Hamiltonian. In addition, $\boldsymbol{\lambda}$ and therefore $\boldsymbol{p}$ must be continuous across the impulses. Because $p < 1$ before and after each impulse, then $\dot{p} = 0$ at those points (this includes the final impulse because t_n is free and must also obey Pontryagin's minimum principle). That is,

$$\dot{\boldsymbol{p}}^T\boldsymbol{p} = 0, \quad \forall\ t = t_i \tag{29}$$

assuming without loss of generality that $t_1 \neq 0$. If $t_1 = 0$ and this condition is not satisfied, then there exists a $t_1 < 0$ that will have a lower cost.

Continuity of the Hamiltonian also requires that $H^+ = H^-$ for each impulse,

$$0 = H^+ - H^- = \boldsymbol{\lambda}^T A(\delta\text{œ}^+ - \delta\text{œ}^-) \quad = \dot{\boldsymbol{\lambda}}^T BB^T\boldsymbol{\lambda}\gamma_i \tag{30}$$

Together, Eqs. (29) and (30) then imply the two conditions

$$(B^T\dot{\boldsymbol{\lambda}})^T(B^T\boldsymbol{\lambda}) = 0, \quad \forall\ t = t_i \tag{31}$$

$$(\dot{B}^T\boldsymbol{\lambda})^T(B^T\boldsymbol{\lambda}) = 0, \quad \forall\ t = t_i \tag{32}$$

In Lawden's primer vector theory, the B matrix is constant and these constraints reduce to the familiar $\dot{p} = 0$ condition. For the final time free problem, the last condition is given by

$$0 = H(t_n) = \boldsymbol{\lambda}_n^T A(t_n)\delta\text{œ}_f = -\dot{\boldsymbol{\lambda}}_n^T\delta\text{œ}_f \tag{33}$$

where $\boldsymbol{\lambda}_n = \boldsymbol{\lambda}(t_n)$. This implies that the optimal final time occurs when the derivative of the costate is perpendicular to the desired state (or, equivalently, when the costate is perpendicular to the derivative of the desired state).

2. Computation Difficulties

The continuous-time optimal control problem is challenging to solve because of the nonlinearity of the problem. When the necessary conditions are applied, the result is a set of coupled nonlinear differential equations. Even if the state and costate dynamics are enforced explicitly, these still result in a set of coupled nonlinear algebraic equations. Techniques exist in the literature to solve this problem using the traditional primer vector formulation (e.g., [1,47,48,50,51]) by beginning with two impulses and adding additional ones until the optimal maneuver is obtained. However, these techniques do not apply directly to the present problem because the primer vector now depends on all six elements of the costate through the time-varying GVEs and it is more challenging to obtain a compatible initial estimate for the costate, especially when adding an additional impulse. Furthermore, all of these techniques require a multidimensional nonlinear solver, which will be subject to convergence and multiple solution issues, and it simply may not be practical to implement such an algorithm onboard a small spacecraft.

B. Discrete-Time Optimal Control Problem

Instead of expressing the minimum-fuel problem in terms of the continuous dynamics, it can be stated as a discrete-time optimal problem:

$$J_d = \frac{1}{2}\sum_{k=1}^{N} \boldsymbol{u}_k^T \boldsymbol{u}_k \tag{34}$$

subject to the discrete dynamics

$$\delta\boldsymbol{\varpi}_{k+1} = \boldsymbol{\Phi}_k \delta\boldsymbol{\varpi}_k + \boldsymbol{\Gamma}_k \boldsymbol{u}_k \tag{35}$$

where

$$\boldsymbol{\Phi}_k = \boldsymbol{\Phi}(t_{k+1}, t_k) \tag{36}$$

$$\boldsymbol{\Gamma}_k = \boldsymbol{\Phi}(t_{k+1}, t_k) B(t_k) \tag{37}$$

for impulsive control. The STM defined in Eq. (10) is $\boldsymbol{\Phi}(t_{k+1}, t_k)$. The cost in Eq. (34) is the sum of the squares of the impulse magnitudes at the N discretization points, which is slightly different than the cost in Eq. (22). However, if $N = n$ and the t_k were placed at the optimal times t_i, then minimizing Eq. (34) would be equivalent to minimizing Eq. (22).

A number of previous authors have also used discrete-time formulations such as this to address the reconfiguration problem (e.g., [14,16,17,19–22]). Most of these arrive at different solutions because they use different cost functions, make simplifying assumptions about the reference orbit, or use alternate methods to derive the thrust input or optimality conditions. However, some of them do arrive at the same solution under certain conditions and choices of thrust times. The main difference in this paper compared with previous methods is that the discrete formulation is solved iteratively so that the thrust times converge to the optimal times of the continuous formulation.

1. Necessary Conditions for Optimality

The Hamiltonian for the discrete-time problem is

$$H_d = \frac{1}{2}\boldsymbol{u}_k^T \boldsymbol{u}_k + \boldsymbol{\Lambda}_{k+1}^T (\boldsymbol{\Phi}_k \delta\boldsymbol{\varpi}_k + \boldsymbol{\Gamma}_k \boldsymbol{u}_k) \tag{38}$$

For an optimal control sequence, the costate equation is

$$\boldsymbol{\Lambda}_k = H^d_{\delta\boldsymbol{\varpi}_k} = \boldsymbol{\Phi}_k^T \boldsymbol{\Lambda}_{k+1} \tag{39}$$

The optimal control is given by the stationary condition

$$0 = H^d_{\boldsymbol{u}_k} = \boldsymbol{u}_k + \boldsymbol{\Gamma}_k^T \boldsymbol{\Lambda}_{k+1} \tag{40}$$

$$\boldsymbol{u}_k = -\boldsymbol{\Gamma}_k^T \boldsymbol{\Lambda}_{k+1} \tag{41}$$

Because $\boldsymbol{\Phi}_k$ is invertible, the combined state–costate system can be written as

$$\underbrace{\begin{bmatrix} \delta\boldsymbol{\varpi}_k \\ \boldsymbol{\Lambda}_k \end{bmatrix}}_{z_k} = \underbrace{\begin{bmatrix} \boldsymbol{\Phi}_k^{-1} & B_k B_k^T \boldsymbol{\Phi}_k^T \\ \boldsymbol{0} & \boldsymbol{\Phi}_k^T \end{bmatrix}}_{\Psi_k} \underbrace{\begin{bmatrix} \delta\boldsymbol{\varpi}_{k+1} \\ \boldsymbol{\Lambda}_{k+1} \end{bmatrix}}_{z_{k+1}} \tag{42}$$

where $B_k = B(t_k)$ ([49] Chapter 2). Proceeding backward in time, the solution to Eq. (42) is

$$\boldsymbol{z}_1 = \boldsymbol{\Xi}_{1,N+1} \boldsymbol{z}_{N+1} \tag{43}$$

defining

$$\boldsymbol{\Xi}_{1,N+1} = \begin{bmatrix} \boldsymbol{\xi}_{11} & \boldsymbol{\xi}_{12} \\ \boldsymbol{\xi}_{21} & \boldsymbol{\xi}_{22} \end{bmatrix} = \prod_{k=1}^{N} \boldsymbol{\Psi}_k \tag{44}$$

Expanding the first component of $\boldsymbol{z}_1$ gives

$$\delta\boldsymbol{\varpi}_1 = \boldsymbol{\Phi}(t_1, 0)\delta\boldsymbol{\varpi}_0 = \boldsymbol{\xi}_{11}\delta\boldsymbol{\varpi}_f + \boldsymbol{\xi}_{12}\boldsymbol{\Lambda}_{N+1} \tag{45}$$

where $\delta\boldsymbol{\varpi}_1 = \delta\boldsymbol{\varpi}(t_1)$, because the first impulse does not necessarily occur at $t = 0$. Note that the desired state in the discrete formulation is specified at t_{N+1}. Assuming $\boldsymbol{\xi}_{12}$ is invertible, $\boldsymbol{\Lambda}_{N+1}$ can then be written in terms of the initial and desired final state:

$$\boldsymbol{\Lambda}_{N+1} = \boldsymbol{\xi}_{12}^{-1} \underbrace{[\boldsymbol{\Phi}(t_1, 0)\delta\boldsymbol{\varpi}_0 - \boldsymbol{\xi}_{11}\delta\boldsymbol{\varpi}_f]}_{\Theta} \tag{46}$$

2. Matrix Singularities

Note that, because the unperturbed STM contains orbit-periodic terms with in-plane and out-of-plane motion decoupled, there will be cases when $\boldsymbol{\xi}_{12}$ is singular for certain thrust times if only two impulses are used (or nearly singular for perturbed orbits). In these cases, not all components of the final costate are uniquely determined by Eq. (45), and a minimum-norm solution for $\boldsymbol{\Lambda}_{N+1}$

$$\boldsymbol{\Lambda}_{N+1} = \boldsymbol{\xi}_{12,m}^T (\boldsymbol{\xi}_{12,m} \boldsymbol{\xi}_{12,m}^T)^{-1} \boldsymbol{\Theta}_m \tag{47}$$

will give the optimal control, where $\boldsymbol{\xi}_{12,m}$ and $\boldsymbol{\Theta}_m$ have had their linearly dependent equations removed, such that $\boldsymbol{\xi}_{12,m}$ has full row rank $m < 6$ ([52] Appendix A). However, if the thrust times are nowhere near the continuous optimal thrust times t_i, the solution may not be practically feasible (i.e., it could result in unrealistically large impulses).

IV. Design of Computationally Efficient Algorithm for Onboard Maneuver Targeting

The solution to the minimum-fuel n-impulse maneuver problem is given by the continuous-time optimal control formulation, rather than the discrete formulation, in general. This is because the thrust times in the discrete formulation are specified a priori by the choice of discretization times. If a fine discretization time spacing is used, the optimal thrust times may be found but more thrusts will occur than necessary because the control is determined by the costate that evolves according to the continuous dynamics and cannot simply become zero for several time steps when the optimal trajectory should have a coast arc.

However, the discrete-time optimal control problem is relatively simple to solve: It involves a number of large matrix multiplications and the inversion of a 6×6 matrix. The key to designing a computationally efficient algorithm for onboard maneuver targeting is recognizing the link between the discrete and continuous formulations. Because the state transition matrix solution to the dynamics is known explicitly and the control is impulsive, there is no need for the discretization times to be close together or equally spaced, and the final time t_{N+1} can be arbitrarily chosen to be the same as the final control time t_N. As mentioned previously, if the t_k are placed exactly at the optimal times t_i, then the discrete optimal control sequence is also optimal in the continuous formulation.

In that case, the control at each t_i is the same in both the continuous and discrete formulations:

$$\boldsymbol{u}_i = -B_i^T \boldsymbol{\Phi}^T(t_n, t_i)\boldsymbol{\Lambda}_n = -\gamma_i B_i^T \boldsymbol{\Phi}^T(t_n, t_i)\boldsymbol{\lambda}_n \tag{48}$$

since $\boldsymbol{\Lambda}_{N+1} = \boldsymbol{\Lambda}_N$, $N = n$, and $B_i = B(t_i)$. Evaluating this equation at each control time, $\boldsymbol{\lambda}_n$ can then be found by solving the linear system

$$\begin{bmatrix} -\gamma_1 B_1^T \boldsymbol{\Phi}^T(t_n, t_1) \\ -\gamma_2 B_2^T \boldsymbol{\Phi}^T(t_n, t_2) \\ \vdots \\ -\gamma_n B_n^T \end{bmatrix} \boldsymbol{\lambda}_n = \begin{bmatrix} \boldsymbol{u}_1 \\ \boldsymbol{u}_2 \\ \vdots \\ \boldsymbol{u}_n \end{bmatrix} \tag{49}$$

This system is guaranteed to have an exact solution because all of the necessary conditions for optimality of the continuous formulation are satisfied under these assumptions.

A. Criteria for Improving a Suboptimal Trajectory

If the t_k are not placed at the optimal times, then the discrete optimal control sequence will not be optimal in the continuous formulation, but it will still represent a feasible solution because it satisfies the final state constraint. In this case, Eq. (49) may not have an exact solution. However, if the t_k are close to the optimal times, then a least-squares solution of Eq. (49) will give an approximation of the final costate, but it will not satisfy the necessary conditions for optimality. By examining the resulting primer vector magnitude history it is possible to use the analysis of Lawden [23], Lion and Handelsman [50], and Jezewksi and Rozendaal [51] to improve the trajectory. That analysis identifies two important criteria for improving a suboptimal trajectory:

1) Moving an impulse: If $\dot{p} \neq 0$ at any impulse, move the impulse time slightly in the direction of increasing p.
2) Adding an impulse: If $p > 1$ somewhere other than near an impulse, add another impulse at the time of maximum p.
3) However, those methods always begin with two impulses and add more as required for optimality, whereas this algorithm may begin with a suboptimal solution with too many impulses. Therefore, one additional criterion is defined for removing an impulse:
   Removing an impulse: If $p < 1$ and $\dot{p} = 0$ at any impulse, remove the impulse.

The improved trajectory is determined by resolving the discrete optimal control problem with the new impulse times t_k. In any case, the maximum number of impulses required for the optimal maneuver is six. This is determined from a result by Neustadt [53] and Potter and Stern [54], which states that, for a linear system, the maximum number of impulses necessary to realize an optimal transfer is the number of constraints on the state variables at the final time. Practically speaking, four impulses are usually sufficient for an in-plane maneuver, because the out-of-plane coupling is of $\mathcal{O}(J_2)$.

B. Initial Estimate for Optimal Thrust Times

To obtain an initial estimate for the optimal thrust times, solve the discrete optimal control problem using a large number of impulses (e.g., 12 or more). Note that the total maneuver duration used to generate the initial estimate is implicitly assumed to be the approximate maximum maneuver duration. The final solution obtained using this algorithm is a local optimum in the vicinity of this maneuver duration. That is, the final optimal maneuver may have a duration of less than or slightly greater than the original duration, but the algorithm will not find optimal maneuvers with durations multiple orbits greater than the initial estimate. For maneuvers without large along-track (i.e., anomaly) changes, one to two orbits are typically a sufficient duration. For pure along-track maneuvers, or maneuvers with large along-track changes, the optimal maneuver duration is actually infinite, and so the maximum maneuver duration must instead be dictated by mission constraints; this algorithm then finds the closest locally optimal maneuver (see Sec. V for an example of a pure along-track maneuver).

After solving the discrete optimal control problem using a large number of impulses, examine the resulting impulse magnitude history and select the times of any local maxima as estimates for the optimal thrust times. This technique quickly identifies the likely optimal number of impulses, and it eventually converges to the continuous-time optimal solution. In practice, though, it may not be necessary to determine the optimal thrust times exactly. Thrust magnitude and alignment errors, minimum impulse limits, finite thrust approximations, onboard navigation and timing inaccuracies, and other error sources mean that there is a point at which the improvement in going from a suboptimal to an optimal trajectory is below the threshold realizable by the actual system. Therefore, it is possible to define an algorithm that incrementally improves a suboptimal trajectory until the improvement in fuel cost (or the changes in thrust application times) is below some threshold, at which point the problem is considered "solved." The solution is the optimal number of impulses n, their application times $\{t_1, t_2, \ldots, t_n\}$, and the final costate $\mathbf{\Lambda}_{N+1}$ that yields the optimal impulses through Eqs. (39) and (41).

For example, the impulse magnitude history for a 24-impulse in-plane reconfiguration is shown in Fig. 2 (for a circular, unperturbed reference orbit). The optimal number of impulses appears to be three and the candidate optimal thrust times (t_1, t_2, and t_3) are identified at the peak impulse locations. After resolving the discrete problem using the new impulse times, the least-squares solution of Eq. (49) results in the primer magnitude history shown in Fig. 3, with the impulse locations indicated as circles (note that the primer magnitude at each impulse is not exactly equal to one, as expected). The preceding criteria indicate that the trajectory can be improved by slightly decreasing t_1 and t_2 and increasing t_3, which results in the refined primer magnitude history shown in Fig. 4 once the discrete

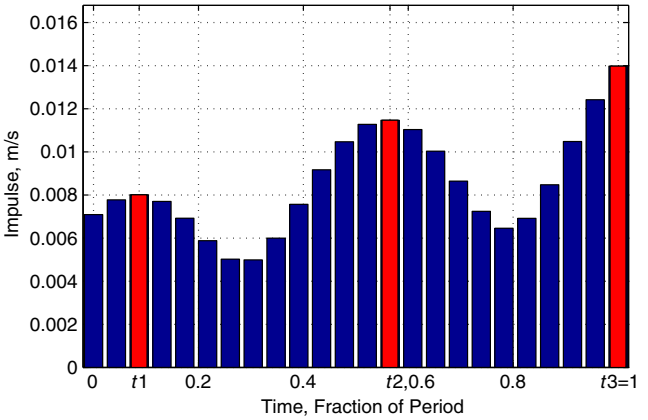

Fig. 2 Impulse magnitudes for 24-impulse maneuver, identifying candidate optimal impulse times.

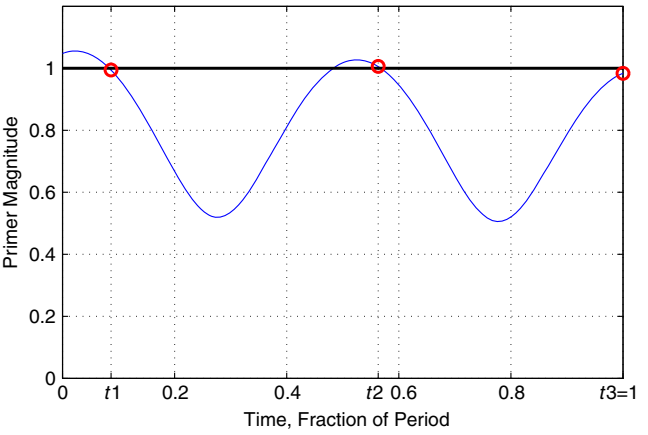

Fig. 3 Primer history for suboptimal three-impulse maneuver using candidate optimal impulse times.

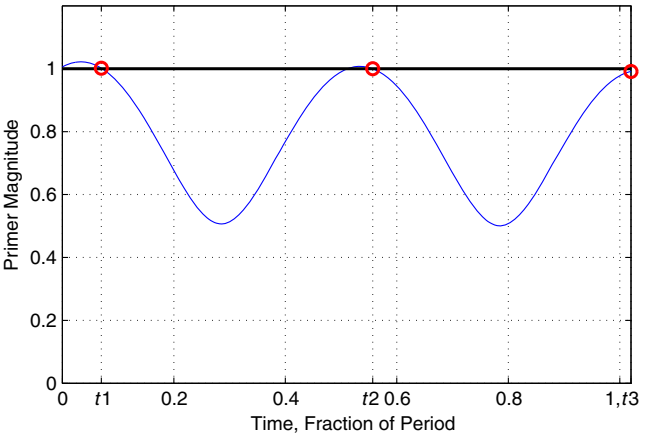

Fig. 4 Primer history for partly refined suboptimal three-impulse maneuver.

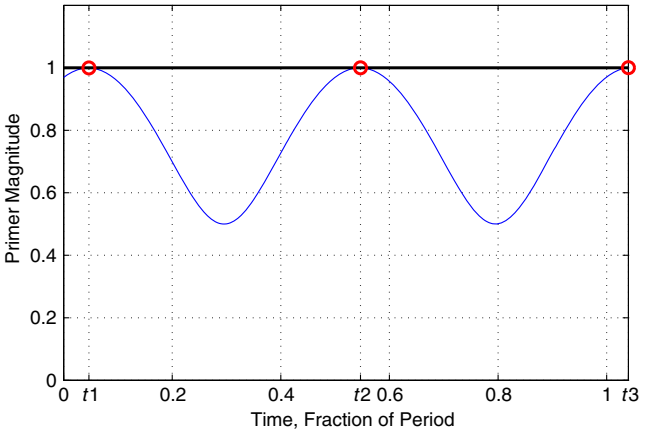

Fig. 5 Primer history for optimal three-impulse maneuver.

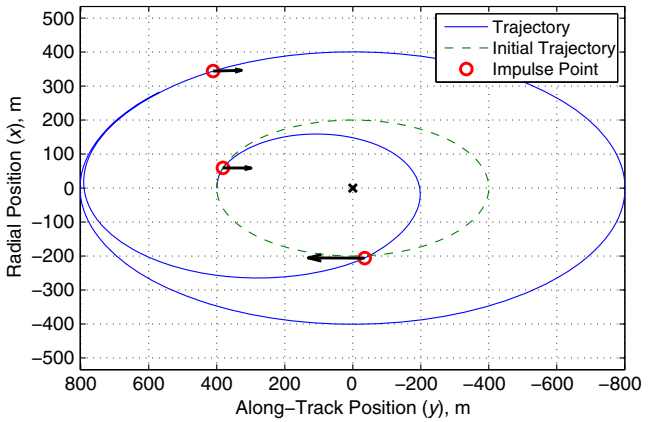

Fig. 6 Optimal planar three-impulse maneuver, $e = 0$.

problem has been resolved. Continuing to refine the thrust times in this fashion eventually results in the optimal primer magnitude history of Fig. 5, which corresponds to the trajectory shown in Fig. 6. The total ΔV fuel cost required for each of these iterations is listed in Table 1 along with the corresponding two-impulse solution from Vaddi et al. [14].

C. Algorithm Summary

In summary, the algorithm can be implemented as follows:

1) Generate an initial candidate primer magnitude history.
   a) Solve Eq. (46) using 12 or more impulse times.
   b) Determine the impulse history using Eqs. (39) and (41).
   c) Examine the impulse magnitudes and determine the times of any local maxima. These are the initial candidate impulse times $\{t_1, \ldots, t_n\}$.
   d) Resolve Eqs. (46), (39), and (41) using the times from the previous step.
   e) Solve Eq. (49) for $\boldsymbol{\lambda}_n$.
   f) Determine the primer magnitude history from Eqs. (25) and (26).
2) Apply the criteria for improving a suboptimal trajectory identified in Sec. IV.A to update the impulse times $\{t_1, \ldots, t_n\}$.
3) Resolve Eqs. (46), (39), and (41) using the updated impulse times.
4) Solve Eq. (49) for $\boldsymbol{\lambda}_n$.
5) Determine the updated primer magnitude history from Eqs. (25) and (26).
6) Evaluate the primer magnitude history for optimality (convergence condition).
7) Repeat steps 2–6 until convergence.

This algorithm is more computationally efficient than attempting to solve the continuous-time optimal control problem directly because it requires only matrix multiplications and the solution of two linear systems of equations at each iteration. State and costate propagation is performed using the Gim-Alfriend STM, which is defined analytically, and does not require any numerical integration. In addition, the iteration can be terminated before convergence and still return a useful solution because every suboptimal set of impulses represents a feasible solution (i.e., it satisfies the boundary conditions) to the reconfiguration problem. In practice, alternate algorithm convergence conditions can be used: For example, if the improvement in total fuel cost from one iteration to the next is small, terminate the iteration even if the optimality conditions are not satisfied. This also means that if the algorithm needs to be terminated due to a maximum allowable number of iterations, the final solution can still be used if the total fuel cost is acceptable.

V. Simulation Results

Next, the ability of the algorithm of Sec. IV to target general reconfiguration maneuvers is demonstrated. Several example maneuvers are considered for circular and elliptic orbits, with and without J_2. Maneuvers planned with J_2 included in the dynamics are simulated with J_2–J_6. Example maneuvers are also simulated for the reference orbit of the CPOD mission.

A. Circular Orbit

Circular orbits are an important case to consider for any formation flying algorithm because of the breadth of interest in the aerospace community for applications and theory in such orbits. Classical orbital element methods fall short in this respect because the reference orbit parameters become singular for $e = 0$, reducing to a set of five independent quantities, whereas the deputy still requires six quantities to describe its relative orbit. Because this paper uses the nearly nonsingular elements, the algorithm described here is uniformly applicable to both circular and elliptic orbits without modification (except when $i = 0$). The first circular orbit example is described in the preceding section, a reconfiguration from a $\rho_1 = 200$ m, $\tilde{\alpha}_0 = 0$ in-plane ellipse to a $\rho_1 = 400$ m, $\tilde{\alpha}_0 = \pi/4$ in-plane ellipse, simulated without perturbations. The reference mean orbital elements are listed in Table 2 (circular case).

1. *Pure Along-Track Maneuver*

Another important case to consider is a reconfiguration between two leader–follower formations, a pure along-track or anomaly change, also known as a "V-bar maneuver." This maneuver is challenging to design because the optimal maneuver times are spaced infinitely far apart. This is because the optimal maneuver uses the natural anomaly drift of the dynamics to create the desired anomaly change by introducing a small semimajor axis difference. For example, considering only tangential thrust, the optimal two-impulse maneuver is

Table 1 Total fuel cost for maneuver

Maneuver	ΔV, m/s
Two-impulse from [14]	0.3316
24-impulse	0.2050
Suboptimal three-impulse	0.1694
Partly refined three-impulse	0.1669
Optimal three-impulse	0.1658

Table 2 Reference mean orbital elements

Orbital element	Circular	Elliptic
a, km	6803.1366	15,000
λ_0, deg	0	120
i, deg	97.04	45
q_1	0	-0.25
q_2	0	0.43301
Ω, deg	270.828	90

$$\Delta V_1 = -\frac{1}{3}\frac{\Delta d}{N_{\text{orb}} T} = -\Delta V_2 \tag{50}$$

where ΔV_1 and ΔV_2 are the two tangential impulses, spaced an integer number N_{orb} of orbit periods T apart, and Δd is the desired change in along-track position. Because the total fuel cost is inversely proportional to the duration, the optimal maneuver has an infinitesimal fuel cost and infinite duration.

However, this algorithm still finds the suboptimal maneuver for a given maneuver duration. The optimal primer histories for the two- and five-orbit cases of a 100 m along-track maneuver are shown in Fig. 7, and the resulting maneuver trajectories are shown in Fig. 8. The primer in the two-orbit case satisfies the necessary conditions for optimality, but extrapolating the primer magnitude into the future clearly shows that it is not globally optimal. The same would be seen if the primer magnitude in the five-orbit case was extrapolated as well. Note that the (locally) optimal maneuver times are not spaced precisely an integer number of orbits apart because the optimal thrusts have a small radial component as well, as shown in the magnified plots of Fig. 8. The fuel cost for the five-orbit maneuver is 2.387 mm/s, whereas the cost for a purely tangential five-orbit maneuver is 2.4 mm/s. The cost for the two-orbit maneuver is 5.967 mm/s.

2. *Out-of-Plane Maneuver*

Next, out-of-plane motion is added and a maneuver is designed to reconfigure a formation from a $\rho_1 = 200$ m, $\tilde{\alpha}_0 = 0$ in-plane ellipse to a $\rho_1 = 400$ m, $\tilde{\alpha}_0 = \pi/4$, $\rho_3 = 200$ m, $\tilde{\beta}_0 = 3\pi/4$ formation (referred to as a safety ellipse), in a circular orbit with J_2 included in the dynamics. An initial estimate for the candidate optimal thrust times is obtained from the discrete-time optimal impulse profile in Fig. 9. The iterative refinement of the primer history is shown in Fig. 10, which results in a three-impulse optimal maneuver.

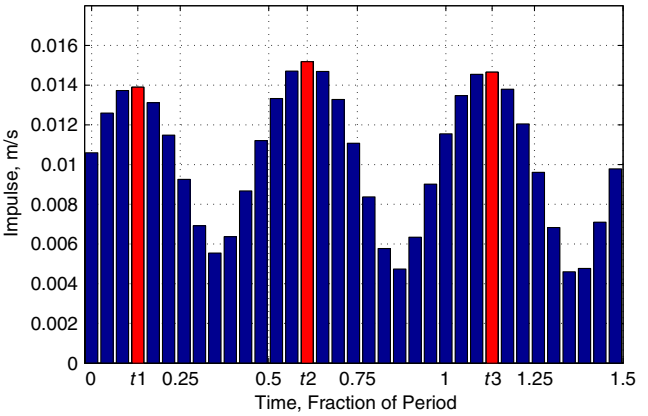

Fig. 9 Impulse magnitudes for maneuver to safety ellipse, identifying candidate optimal impulse times.

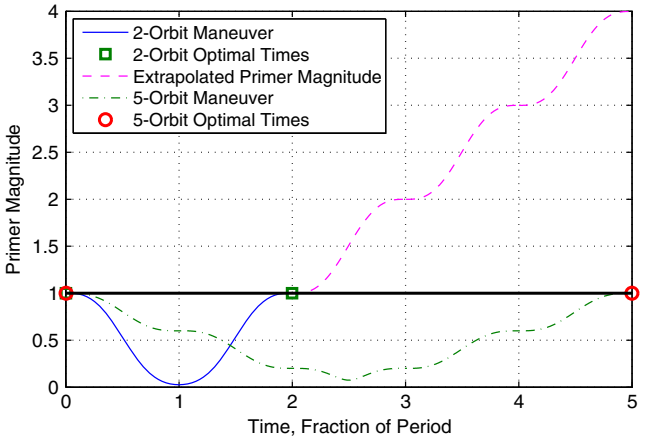

Fig. 7 Primer history for pure along-track maneuver.

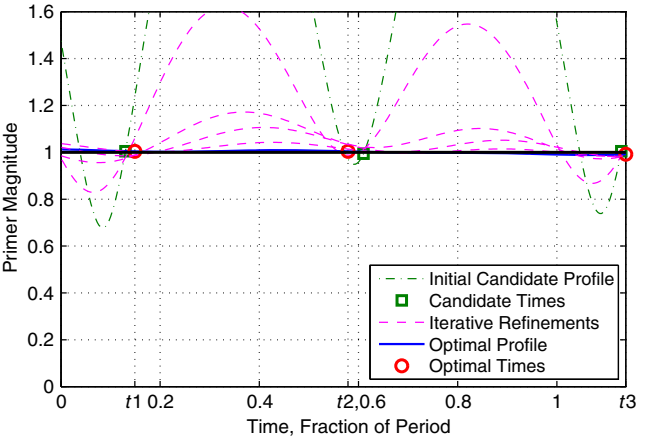

Fig. 10 Primer history for maneuver to safety ellipse.

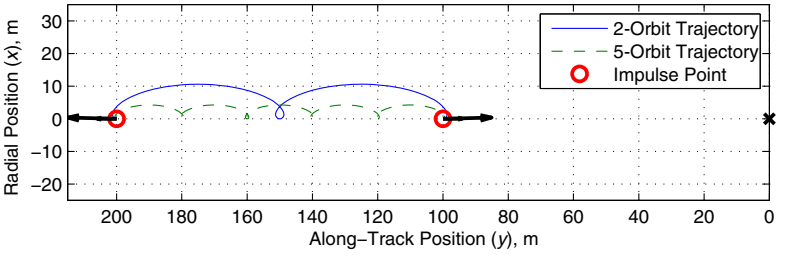

a) LVLH relative position

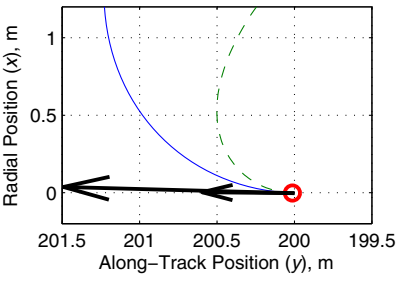

b) Magnified view of impulse

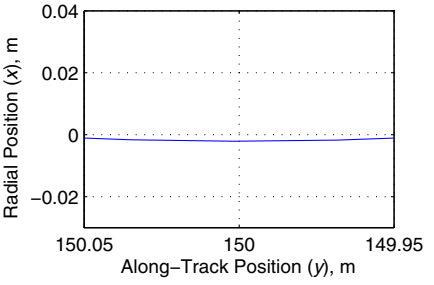

c) Magnified view of midpoint

Fig. 8 Two- and five-orbit along-track maneuver, $e = 0$.

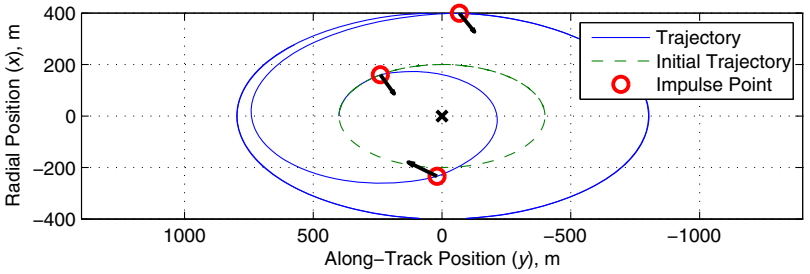

a) LVLH relative position (in-plane)

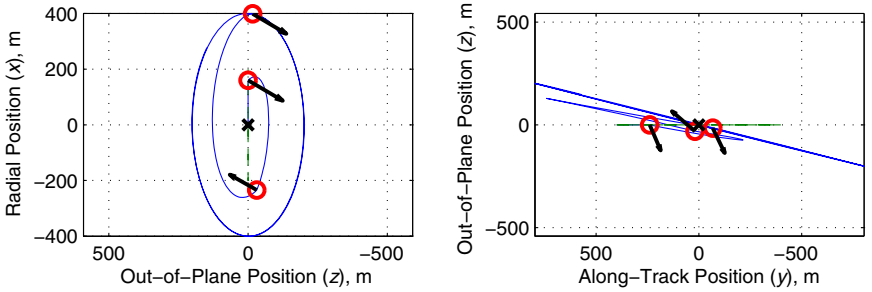

b) Out-of-plane vs radial **c) Along-track vs out-of-plane**

Fig. 11 Optimal three-impulse maneuver to safety ellipse, $e = 0$ with J_2–J_6.

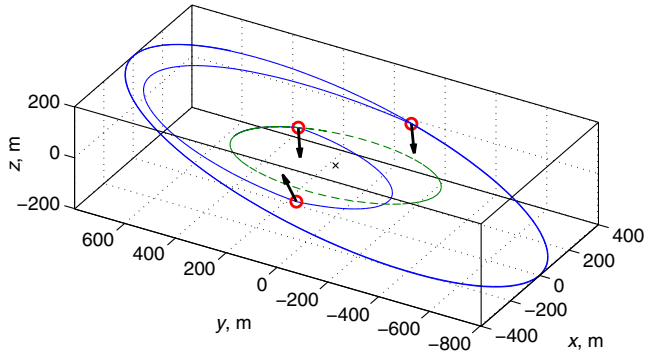

Fig. 12 Optimal three-impulse maneuver to safety ellipse, $e = 0$ with J_2–J_6.

In this case, the optimal primer magnitude is equal to one for the entire maneuver, which is still a valid solution of the degenerate type discussed by Prussing [1]. The optimal thrust times cannot be immediately identified by examining the final primer history, but they are still determined by this algorithm because it converges to the optimal times from a series of compatible suboptimal solutions. The optimal three-impulse trajectory is shown in Figs. 11 and 12 and the total fuel cost for the maneuver is 0.3093 m/s. Using the method of Vaddi et al. [14], the three-impulse fuel cost is 0.5566 m/s.

3. *Comparison to the Method of Anderson and Schaub [21]*

The same maneuver to reconfigure a formation from a $\rho_1 = 200$ m, $\tilde{\alpha}_0 = 0$ in-plane ellipse to a $\rho_1 = 400$ m, $\tilde{\alpha}_0 = \pi/4$, $\rho_3 = 200$ m, $\tilde{\beta}_0 = 3\pi/4$ safety ellipse is now generated using the method of Anderson and Schaub [21]. That method, which is designed for general formation flying applications including those in

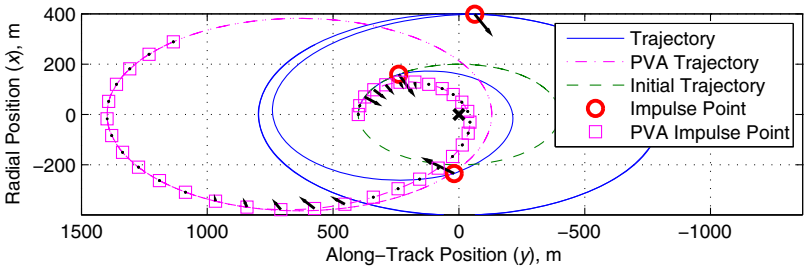

a) LVLH relative position (in-plane)

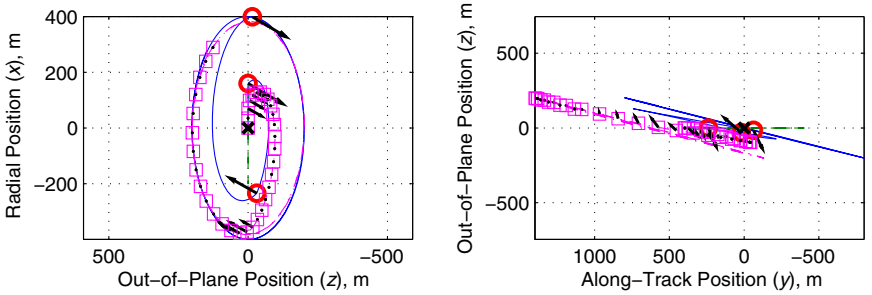

b) Out-of-plane vs radial **c) Along-track vs out-of-plane**

Fig. 13 Thirty-six-impulse maneuver to safety ellipse compared with optimal three-impulse maneuver.

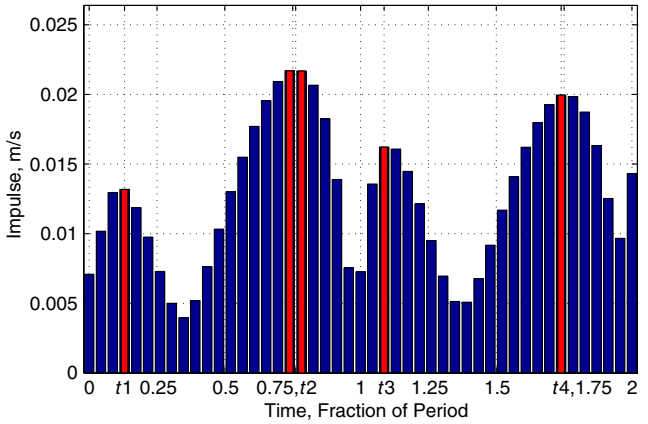

Fig. 14 Impulse magnitudes for maneuver to V-bar, $e = 0.5$, identifying candidate optimal impulse times.

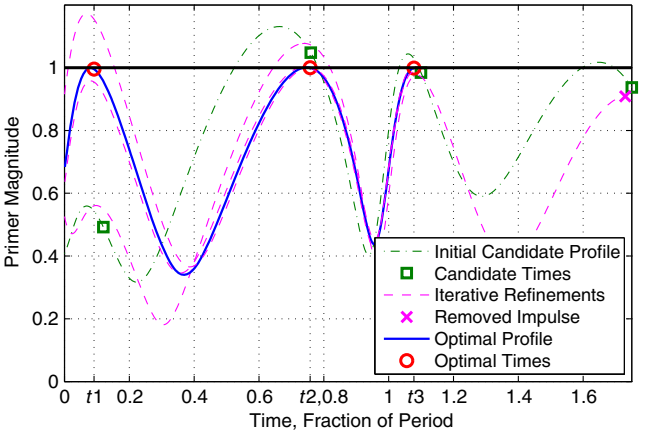

Fig. 15 Primer history for maneuver to V-bar, $e = 0.5$.

the geostationary regime, uses a discretized approximation to generate a near-fuel-optimal impulsive control sequence with impulses applied at equal spacings in true anomaly. The method is applicable in general circular, elliptic, and equatorial orbits because it uses a set of completely nonsingular elements that does not suffer from the same $i = 0$ singularity as the nearly nonsingular element set used in this paper.

Using an anomaly discretization of 10 deg, the resulting 36-impulse trajectory is shown in Fig. 13 (labeled "PVA Trajectory"), along with the optimal three-impulse trajectory of the previous example. In the formulation of Anderson and Schaub [21], the anomaly parameter is not directly controllable, which is the reason for the along-track discrepancy between the two trajectories. The main goal of that method is to reach a formation with a desired size and orientation without specifying a target anomaly. The total fuel cost for the 36-impulse maneuver is 0.3106 m/s, compared with 0.3093 m/s for the optimal three-impulse maneuver.

B. Elliptic Orbit

As mentioned previously, the algorithm presented in this paper is also applicable to formations in elliptic reference orbits, with no approximations or loss of fidelity. To demonstrate, the next simulation shows the design of a maneuver in a reference orbit with an eccentricity of $e = 0.5$, from a $\rho_1 = 1$ km, $\tilde{\alpha}_0 = \pi/4$, $\rho_3 = 1$ km, $\tilde{\beta}_0 = 3\pi/4$ eccentric safety ellipse to a $\rho_2 = 1$ km average V-bar position. The actual TH parameters are defined using the eccentric modifications described by Sengupta and Vadali [29]. The reference mean orbital elements are listed in Table 2 (elliptic case).

An initial estimate for the candidate optimal thrust times is obtained from the discrete-time optimal impulse profile in Fig. 14. The iterative refinement of the primer history is shown in Fig. 15, which

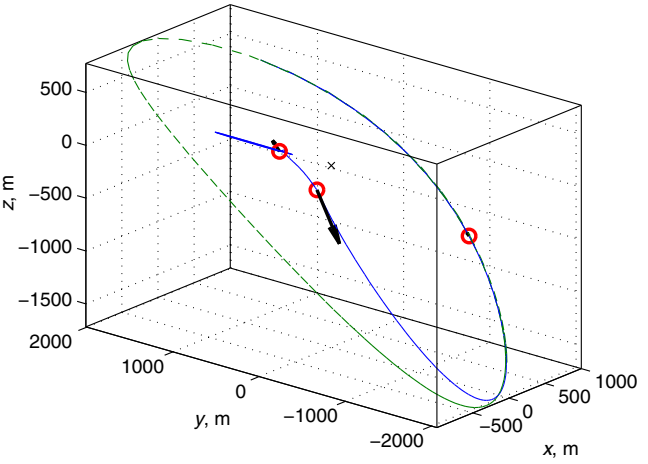

Fig. 17 Optimal three-impulse maneuver to V-bar, $e = 0.5$ with J_2–J_6.

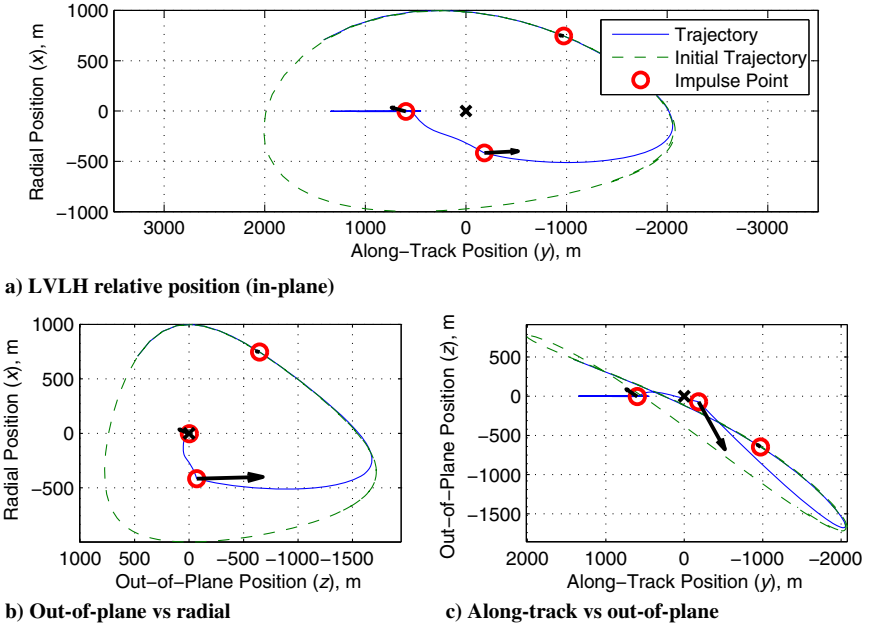

a) LVLH relative position (in-plane)

b) Out-of-plane vs radial

c) Along-track vs out-of-plane

Fig. 16 Optimal three-impulse maneuver to V-bar, $e = 0.5$ with J_2–J_6.

Table 3 CPOD reference mean orbital elements

Orbital element	Value
a, km	6803.1366
λ_0, deg	0
i, deg	97.04
q_1	0.005
q_2	0
Ω, deg	270.828

results in the three-impulse optimal maneuver shown in Figs. 16 and 17. In this case, the initial candidate maneuver has four impulses, but one is removed during the iterative refinement. In fact, the algorithm initially removed the first impulse but then failed to converge to an optimal primer profile, and so the impulse was added back and the final impulse was removed instead. This illustrates one of the primary advantages of this algorithm, which is that each iteration of the solution represents a feasible control trajectory, even if it does not satisfy the continuous-time optimality conditions. Therefore, even if the algorithm had failed to correct the initial candidate maneuver, the resulting set of impulses would still accomplish the desired maneuver. In this case, the difference in fuel cost between the two trajectories was small. The total fuel cost for the maneuver is 0.4559 m/s.

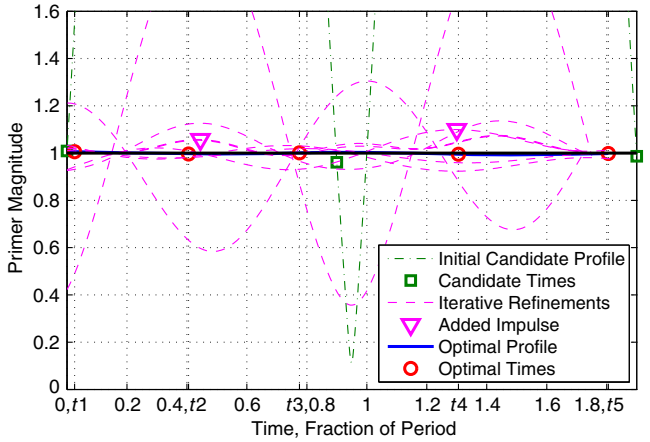

Fig. 18 Primer history for CPOD maneuver to initiate walking safety ellipse.

C. CPOD Maneuvers in Near-Circular Orbit

The NASA CPOD mission is designed to perform rendezvous, proximity operations, and docking with a pair of identical three-unit CubeSats and is currently scheduled for launch in the fall of 2015. The mission baseline is modeled as a near-circular ($e = 0.005$), 425 km sun-synchronous orbit (reference mean orbital elements are listed in Table 3). The maneuver targeting algorithm presented here is to be used as the basis of the CPOD guidance system. The mission

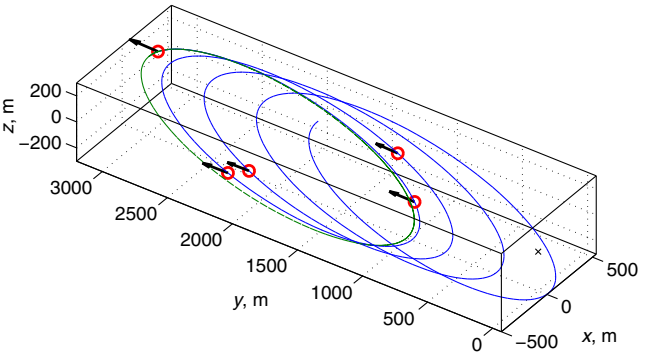

Fig. 20 Optimal five-impulse CPOD maneuver to initiate walking safety ellipse with J_2–J_6.

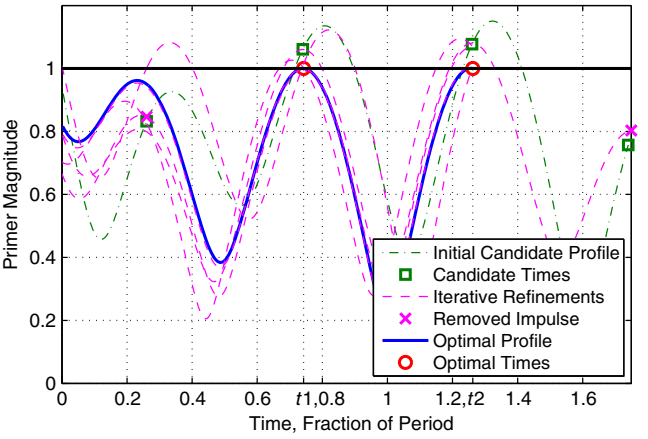

Fig. 21 Primer history for CPOD maneuver to safety ellipse.

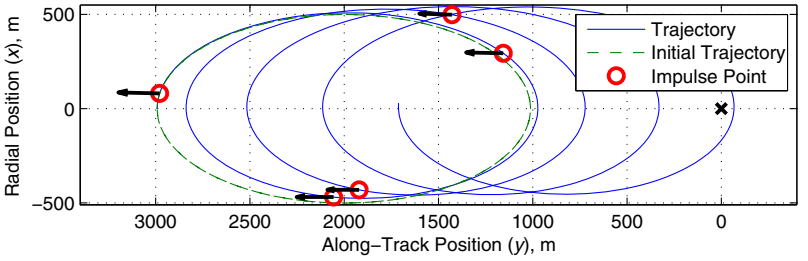

a) LVLH relative position (in-plane)

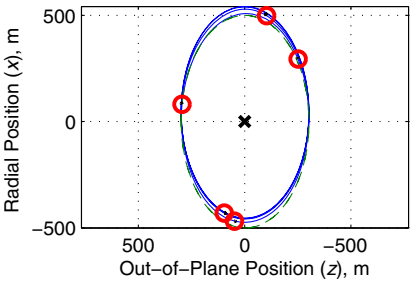

b) Out-of-plane vs radial

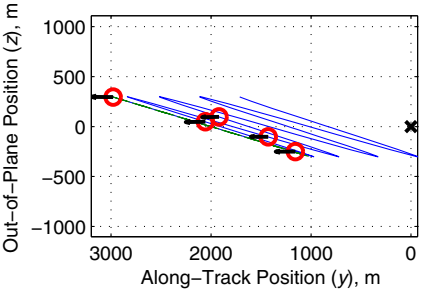

c) Along-track vs out-of-plane

Fig. 19 Optimal five-impulse CPOD maneuver to initiate walking safety ellipse with J_2–J_6.

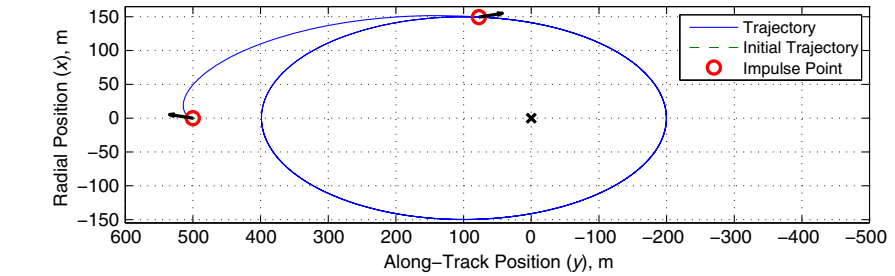

a) LVLH relative position (in-plane)

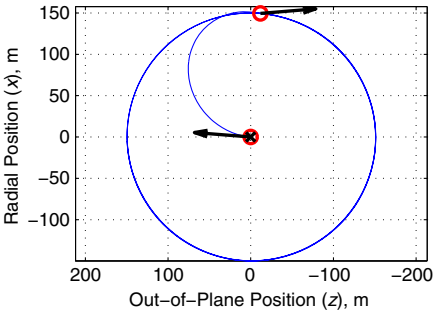

b) Out-of-plane vs radial

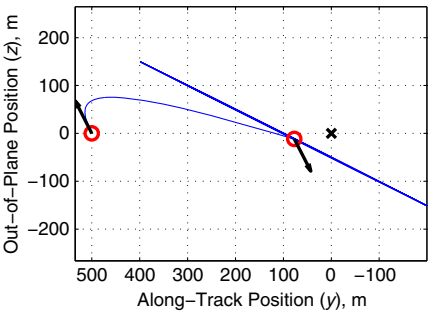

c) Along-track vs out-of-plane

Fig. 22 Optimal two-impulse CPOD maneuver to safety ellipse with J_2–J_6.

will employ passively safe trajectories for rendezvous and standby between active operations.

1. Initiate Walking Safety Ellipse

The first CPOD maneuver simulated in this section is the initiation of a rendezvous trajectory, that is, reconfiguring from a safety ellipse displaced some distance away from the chief to a walking safety ellipse (defined as a safety ellipse with nonzero v_d). In this case, $\rho_1 = 500$ m, $\tilde{\alpha}_0 = 0$, $\rho_3 = 300$ m, $\tilde{\beta}_0 = \pi/2$, $d = 2$ km, and the target $v_d = -400$ m/revolutions. The iterative refinement of the primer history is shown in Fig. 18. The initial candidate maneuver has three impulses and two additional impulses are added, resulting in another solution of the degenerate type in which the optimal primer magnitude is equal to one for the entire maneuver. The final five-impulse optimal maneuver is shown in Figs. 19 and 20, and it has a total fuel cost of 23.87 mm/s.

2. Maneuver to Safety Ellipse

The final maneuver simulated is the initiation of a safety ellipse ($\rho_1 = 150$ m, $\tilde{\alpha}_0 = 0$, $\rho_3 = 150$ m, $\tilde{\beta}_0 = \pi/2$, $d = 100$ m) from a V-bar standoff position ($d = 500$ m). The iterative refinement of the primer history is shown in Fig. 21, which results in a two-impulse optimal maneuver. The resulting two-impulse optimal maneuver is shown in Figs. 22 and 23, and the total fuel cost is 0.1903 m/s.

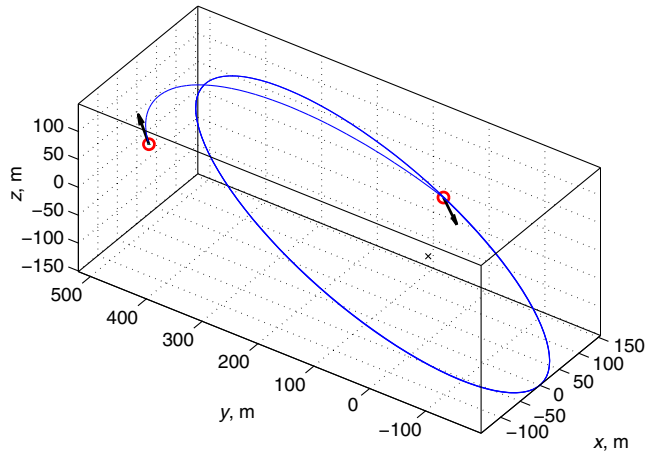

Fig. 23 Optimal two-impulse CPOD maneuver to safety ellipse with J_2–J_6.

VI. Conclusions

The dynamic formulation and optimal control equations presented here provide the information necessary to set up the complete formation reconfiguration algorithm derived in this paper. This algorithm is suitable for implementation onboard a spacecraft with limited processing power because it only involves the solution of linear systems, as opposed to more complex methods that require the solution of nonlinear systems. Fuel-optimal n-impulse reconfiguration maneuvers are designed by iteratively solving a discrete-time maneuver targeting problem, which satisfies the state constraints but does not necessarily use the optimal number of impulses or impulse times, using the continuous-time necessary conditions for optimality to refine the impulse times until they converge to the optimal values. Simulation results show that this method, which is uniformly applicable to both circular and elliptic orbits of nonzero inclination, and includes J_2 effects, produces accurate maneuvers with significantly lower fuel costs than comparable suboptimal, practically implementable methods.

The primary advantages of this algorithm over previous primer vector formulations of the optimal reconfiguration problem are that it does not require the direct solution of the optimal control problem, it includes the effects of eccentricity and J_2, and it produces a feasible solution at each iteration step. However, it still has certain limitations. First, numerical difficulties can be encountered when solving Eq. (49), especially when generating an initial candidate primer vector history and adding or removing impulses. Because this equation is only guaranteed to have an exact solution when the impulse times are optimal, the approximate solution may not be accurate if the impulse times are far from the optimal times. Typically, a poor initial set of candidate impulse times can be improved by changing the total maneuver interval or the initial number of impulses. Second, it does not include any constraints along the reconfiguration trajectory, which would be necessary to enforce close approach requirements, for example. In the CubeSat Proximity Operations Demonstration mission, optimal maneuvers generated by this algorithm need to be checked for close approaches before implementation. Therefore, adding constraints to the optimal control problem will be the subject of future research. Finally, the nearly nonsingular orbital element set

is still singular in the case of equatorial orbits, and it would be desirable to modify the algorithm to use equinoctial elements instead.

Appendix A: Gauss's Variational Equations for Nearly Nonsingular Elements

The nearly nonsingular form of Gauss's Variational Equations (GVEs) is derived from the classical form of Battin [35] using the relationships

$$e\cos f = q_1\cos\theta + q_2\sin\theta \tag{A1}$$

$$e\sin f = q_1\sin\theta - q_2\cos\theta \tag{A2}$$

$$\frac{\eta-1}{he} = \frac{-e}{h(1+\eta)} \tag{A3}$$

$$\eta^2 = 1 - q_1^2 - q_2^2 \tag{A4}$$

In terms of nearly nonsingular elements, the orbit equation is

$$r = \frac{a\eta^2}{1 + q_1\cos\theta + q_2\sin\theta} \tag{A5}$$

The nearly nonsingular form of GVEs is then expressed as

$$\frac{\mathrm{d}a}{\mathrm{d}t} = \frac{2a^2}{h}\left[(q_1\sin\theta - q_2\cos\theta)u_r + \frac{p}{r}u_t\right] \tag{A6}$$

$$\frac{\mathrm{d}\lambda}{\mathrm{d}t} = \left[\frac{-p}{h(1+\eta)}(q_1\cos\theta + q_2\sin\theta) - \frac{2\eta r}{h}\right]u_r + \frac{p+r}{h(1+\eta)}(q_1\sin\theta - q_2\cos\theta)u_t - \frac{r\sin\theta\cos i}{h\sin i}u_h \tag{A7}$$

$$\frac{\mathrm{d}i}{\mathrm{d}t} = \frac{r\cos\theta}{h}u_h \tag{A8}$$

$$\frac{\mathrm{d}q_1}{\mathrm{d}t} = \frac{p\sin\theta}{h}u_r + \frac{1}{h}[(p+r)\cos\theta + rq_1]u_t + \frac{rq_2\sin\theta\cos i}{h\sin i}u_h \tag{A9}$$

$$\frac{\mathrm{d}q_2}{\mathrm{d}t} = \frac{-p\cos\theta}{h}u_r + \frac{1}{h}[(p+r)\sin\theta + rq_2]u_t - \frac{rq_1\sin\theta\cos i}{h\sin i}u_h \tag{A10}$$

$$\frac{\mathrm{d}\Omega}{\mathrm{d}t} = \frac{r\sin\theta}{h\sin i}u_h \tag{A11}$$

The rows of the matrix B comprise the coefficients of u_r, u_t, and u_h for each equation, as in

$$B = [b_{ij}] = \left[\frac{\partial\dot{\text{œ}}_i}{\partial u_j}\right] \tag{A12}$$

Appendix B: Differential Form of Lagrange's Planetary Equations

The Jacobian of the LPEs is formed by populating the columns of A with the partial derivatives with respect to each of the nearly nonsingular mean elements:

$$A = [a_{ij}] = \left[\frac{\partial f_i}{\partial\text{œ}_j}\right] \tag{B1}$$

Defining the constant parameter ϵ as in Schaub et al. [36],

$$\epsilon = J_2\left(\frac{R_e}{p}\right)^2 n \tag{B2}$$

the nonzero elements of A are

$$\frac{\partial f_\lambda}{\partial a} = \frac{-3n}{2a} - \frac{21\epsilon}{8a}[\eta(3\cos^2 i - 1) + (5\cos^2 i - 1)] \tag{B3}$$

$$\frac{\partial f_\lambda}{\partial i} = \frac{-3\epsilon}{4}(3\eta + 5)\sin 2i \tag{B4}$$

$$\frac{\partial f_\lambda}{\partial q_1} = \frac{3\epsilon}{4\eta^2}[3\eta(3\cos^2 i - 1) + 4(5\cos^2 i - 1)]q_1 \tag{B5}$$

$$\frac{\partial f_\lambda}{\partial q_2} = \frac{3\epsilon}{4\eta^2}[3\eta(3\cos^2 i - 1) + 4(5\cos^2 i - 1)]q_2 \tag{B6}$$

$$\frac{\partial f_{q_1}}{\partial a} = \frac{21\epsilon}{8a}(5\cos^2 i - 1)q_2 \tag{B7}$$

$$\frac{\partial f_{q_1}}{\partial i} = \frac{15\epsilon}{4}q_2\sin 2i \tag{B8}$$

$$\frac{\partial f_{q_1}}{\partial q_1} = \frac{-3\epsilon}{\eta^2}(5\cos^2 i - 1)q_1q_2 \tag{B9}$$

$$\frac{\partial f_{q_1}}{\partial q_2} = \frac{-3\epsilon}{4}\left(1 + \frac{4q_2^2}{\eta^2}\right)(5\cos^2 i - 1) \tag{B10}$$

$$\frac{\partial f_{q_2}}{\partial a} = -\frac{21\epsilon}{8a}(5\cos^2 i - 1)q_1 \tag{B11}$$

$$\frac{\partial f_{q_2}}{\partial i} = \frac{-15\epsilon}{4}q_1\sin 2i \tag{B12}$$

$$\frac{\partial f_{q_2}}{\partial q_1} = \frac{3\epsilon}{4}\left(1 + \frac{4q_1^2}{\eta^2}\right)(5\cos^2 i - 1) \tag{B13}$$

$$\frac{\partial f_{q_2}}{\partial q_2} = \frac{3\epsilon}{\eta^2}(5\cos^2 i - 1)q_1 q_2 \tag{B14}$$

$$\frac{\partial f_\Omega}{\partial a} = \frac{21\epsilon}{4a}\cos\, i \tag{B15}$$

$$\frac{\partial f_\Omega}{\partial i} = \frac{3\epsilon}{2}\sin\, i \tag{B16}$$

$$\frac{\partial f_\Omega}{\partial q_1} = \frac{-6\epsilon}{\eta^2} q_1\, \cos\, i \tag{B17}$$

$$\frac{\partial f_\Omega}{\partial q_2} = \frac{-6\epsilon}{\eta^2} q_2\, \cos\, i \tag{B18}$$

Note that the only time-varying quantities in this matrix are q_1 and q_2, whose time derivatives are

$$\dot{q}_1 = -q_2\dot{\omega} \tag{B19}$$

$$\dot{q}_2 = q_1\dot{\omega} \tag{B20}$$

with

$$\dot{\omega} = \frac{3\epsilon}{4}(5\cos^2 i - 1) \tag{B21}$$

on the order of J_2. The solution to these equations is periodic with a period of $\mathcal{O}(J_2^{-1})$,

$$q_1(t) = q_{1,0}\, \cos(\dot{\omega}(t - t_0)) - q_{2,0}\, \sin(\dot{\omega}(t - t_0)) \tag{B22}$$

$$q_2(t) = q_{1,0}\, \sin(\dot{\omega}(t - t_0)) + q_{2,0}\, \cos(\dot{\omega}(t - t_0)) \tag{B23}$$

where $q_{1,0}$ and $q_{2,0}$ are their values at t_0. Therefore, the matrix A is composed of only constant and slowly varying periodic terms.

Appendix C: Solution of the Costate Equation

Consider a system of the form

$$\dot{\boldsymbol{x}} = A(t)\boldsymbol{x} \tag{C1}$$

$$\dot{\boldsymbol{\lambda}} = -A^T(t)\boldsymbol{\lambda} \tag{C2}$$

It turns out that

$$\boldsymbol{x}^T(t)\boldsymbol{\lambda}(t) = \text{constant} \tag{C3}$$

is an invariant of this dynamic system. To show this, differentiate $\boldsymbol{x}^T\boldsymbol{\lambda}$ and substitute Eqs. (C1) and (C2) to find

$$\frac{\mathrm{d}(\boldsymbol{x}^T\boldsymbol{\lambda})}{\mathrm{d}t} = \dot{\boldsymbol{x}}^T\boldsymbol{\lambda} + \boldsymbol{x}^T\dot{\boldsymbol{\lambda}} = \boldsymbol{x}^T A^T(t)\boldsymbol{\lambda} + \boldsymbol{x}^T[-A^T(t)\boldsymbol{\lambda}] = 0 \tag{C4}$$

Next, assume state transition matrices have been developed for both states, yielding

$$\boldsymbol{x}(t_2) = \boldsymbol{\Phi}(t_2, t_1)\boldsymbol{x}(t_1) \tag{C5}$$

$$\boldsymbol{\lambda}(t_2) = \boldsymbol{\phi}(t_2, t_1)\boldsymbol{\lambda}(t_1) \tag{C6}$$

To find the analytical relationship between the STM $\boldsymbol{\phi}(t_2, t_1)$ and $\boldsymbol{\Phi}(t_2, t_1)$, substitute Eqs. (C5) and (C6) into the invariant property in Eq. (C3):

$$\boldsymbol{x}^T(t_1)\boldsymbol{\lambda}(t_1) = \boldsymbol{x}^T(t_2)\boldsymbol{\lambda}(t_2) = \boldsymbol{x}^T(t_1)\underbrace{\boldsymbol{\Phi}^T(t_2, t_1)\boldsymbol{\phi}(t_2, t_1)}_{I_{6\times 6}}\boldsymbol{\lambda}(t_1) \tag{C7}$$

This leads to

$$\boldsymbol{I}_{6\times 6} = \boldsymbol{\Phi}^T(t_2, t_1)\boldsymbol{\phi}(t_2, t_1) \tag{C8}$$

$$\Rightarrow \boldsymbol{\phi}(t_2, t_1) = \boldsymbol{\Phi}^{-T}(t_2, t_1) = \boldsymbol{\Phi}^T(t_1, t_2) \tag{C9}$$

Thus, finally, the STM solution of the $\boldsymbol{\lambda}(t)$ trajectory is

$$\boldsymbol{\lambda}(t_2) = \boldsymbol{\Phi}^T(t_1, t_2)\boldsymbol{\lambda}(t_1) \tag{C10}$$

Acknowledgments

The authors wish to thank John Bowen, Al Tsuda, and Marco Villa of Tyvak Nano-Satellite Systems, Inc. for their support and technical input to this work. Additionally, they thank Paul Anderson of the University of Colorado at Boulder for providing valuable simulation results for comparing this algorithm to the method of Anderson and Schaub [21].

References

[1] Prussing, J. E., "Optimal Four-Impulse Fixed-Time Rendezvous in the Vicinity of a Circular Orbit," *AIAA Journal*, Vol. 7, No. 5, May 1969, pp. 928–935. doi:10.2514/3.5246

[2] Prussing, J. E., "Optimal Two- and Three-Impulse Fixed-Time Rendezvous in the Vicinity of a Circular Orbit," *AIAA Journal*, Vol. 8, No. 7, July 1970, pp. 1221–1228. doi:10.2514/3.5876

[3] Jezewski, D. J., and Donaldson, J. D., "Analytic Approach to Optimal Rendezvous Using Clohessy-Wiltshire Equations," *Journal of Astronautical Sciences*, Vol. 27, July–Sept. 1979, pp. 293–310.

[4] Prussing, J. E., and Chiu, J.-H., "Optimal Multiple-Impulse Time-Fixed Rendezvous Between Circular Orbits," *Journal of Guidance, Control, and Dynamics*, Vol. 9, No. 1, Jan.–Feb. 1986, pp. 17–22. doi:10.2514/3.20060

[5] Carter, T. E., and Humi, M., "Fuel-Optimal Rendezvous near a Point in General Keplerian Orbit," *Journal of Guidance, Control, and Dynamics*, Vol. 10, No. 6, Nov.–Dec. 1987, pp. 567–573. doi:10.2514/3.20257

[6] Shankar, G. S., "Autonomous Guidance Scheme for Orbital Rendezvous," Ph.D. Thesis, Indian Inst. of Science, Bangalore, India, Jan. 1995.

[7] Bell, J. L., "Primer Vector Theory in the Design of Optimal Transfers Involving Libration Point Orbits," Ph.D. Thesis, Purdue Univ., West Lafayette, IN, Dec. 1995.

[8] Mailhe, L. H., Schiff, C., and Folta, D., "Initialization of Formation Flying Using Primer Vector Theory," *International Symposium on Formation Flying Missions and Technology*, CNES, Oct. 2002.

[9] Luo, Y.-Z., Zhang, J., Li, H.-Y., and Tang, G.-J., "Interactive Optimization Approach for Optimal Impulsive Rendezvous Using Primer

Vector and Evolutionary Algorithms," *Acta Astronautica*, Vol. 67, Nos. 3–4, Aug.–Sept. 2010, pp. 396–405. doi:10.1016/j.actaastro.2010.02.014

[10] Aubin, B. S., "Optimization of Relative Orbit Transfers via Particle Swarm and Primer Vector Theory," M.S. Thesis, Univ. of Illinois, Urbana, IL, May 2011.

[11] Huang, W., "Optimal Orbit Transfers for Satellite Formation Flying Applications," Ph.D. Thesis, Univ. of Missouri, Columbia, MO, July 2012.

[12] Arzelier, D., Louembet, C., Rondepierre, A., and Kara-Zaitri, M., "New Mixed Iterative Algorithm to Solve the Fuel-Optimal Linear Impulsive Rendezvous Problem," *Journal of Optimization Theory and Applications*, Vol. 159, No. 1, Oct. 2013, pp. 210–230. doi:10.1007/s10957-013-0282-z

[13] Kim, Y., Park, S.-Y., and Park, C., "Semi-Analytical Global Search Algorithm for Fuel-Optimal Satellite Formation Reconfiguration: Impulsive-Thrust Approach," *Advances in the Astronautical Sciences*, Vol. 150, 2014, pp. 1357–1375; also *Proceedings of the AAS/AIAA Astrodynamics Specialist Conference*, American Astronautical Soc. Paper 13-795, Aug. 2013.

[14] Vaddi, S. S., Alfriend, K. T., Vadali, S. R., and Sengupta, P., "Formation Establishment and Reconfiguration Using Impulsive Control," *Journal of Guidance, Control, and Dynamics*, Vol. 28, No. 2, March–April 2005, pp. 262–268. doi:10.2514/1.6687

[15] Dannemiller, D. P., "Multi-Maneuver Clohessy-Wiltshire Targeting," *Advances in the Astronautical Sciences*, Vol. 142, 2011, pp. 1–14; also *Proceedings of the AAS/AIAA Astrodynamics Specialist Conference*, American Astronautical Soc. Paper 00-012, Feb. 2000.

[16] Saunders, M., "Adaptive Formation Flying Maneuver for Multiple Relative Orbits," M.S. Thesis, Univ. of Colorado, Boulder, CO, Aug. 2011.

[17] Breger, L. S., and How, J. P., "Formation Flying Control for the MMS Mission Using GVE-Based MPC," *Proceedings of the 2005 IEEE Conference on Control Applications*, IEEE, Piscataway, NJ, Aug. 2005, pp. 565–570. doi:10.1109/CCA.2005.1507186

[18] Breger, L. S., and How, J. P., "Gauss's Variational Equation-Based Dynamics and Control for Formation Flying Spacecraft," *Journal of Guidance, Control, and Dynamics*, Vol. 30, No. 2, March–April 2007, pp. 437–448. doi:10.2514/1.22649

[19] Roscoe, C. W. T., "Reconfiguration and Recovery of Formation Flying Spacecraft in Eccentric Orbits," M.A.Sc. Thesis, Univ. of Toronto, Toronto, June 2009.

[20] Roth, N. H., "Navigation and Control Design for the CanX-4/-5 Satellite Formation Flying Mission," M.A.Sc. Thesis, Univ. of Toronto, Toronto, Nov. 2010.

[21] Anderson, P. V., and Schaub, H., "N-Impulse Formation Flying Feedback Control Using Nonsingular Element Description," *Journal of Guidance, Control, and Dynamics*, Vol. 37, No. 2, March–April 2014, pp. 540–548. doi:10.2514/1.60766

[22] Gaias, G., D'Amico, S., and Ardaens, J.-S., "General Multi-Impulsive Maneuver for Optimum Spacecraft Rendezvous," *Fifth International Conference on Spacecraft Formation Flying Missions and Technologies*, DLR, May 2013, Paper 4087.

[23] Lawden, D. F., *Optimal Trajectories for Space Navigation*, Butterworths, London, 1963, pp. 30–124.

[24] D'Amico, S., Ardaens, J.-S., and Montenbruck, O., "Navigation of Formation Flying Spacecraft Using GPS: The PRISMA Technology Demonstration," *Proceedings of the 22nd International Technical Meeting of the Satellite Division of the Institute of Navigation (ION GNSS-2009)*, Institute of Navigation, Manassas, VA, Sept. 2009, pp. 1427–1441.

[25] Roscoe, C. W. T., Griesbach, J. D., Westphal, J. J., Hawes, D. R., and Carrico, J. P., Jr., "Force Modeling and State Propagation for Navigation and Maneuver Planning for CubeSat Rendezvous, Proximity Operations, and Docking," *Advances in the Astronautical Sciences*, Vol. 150, 2014, pp. 573–590; also *Proceedings of the AAS/AIAA Astrodynamics Specialist Conference*, American Astronautical Soc. Paper 13-739, Aug. 2013.

[26] Alfriend, K. T., and Schaub, H., "Dynamics and Control of Spacecraft Formations: Challenges and Some Solutions," *Journal of Astronautical Sciences*, Vol. 48, Nos. 2–3, 2000, pp. 249–267.

[27] Alfriend, K. T., and Yan, H., "Orbital Elements Approach to the Nonlinear Formation Flying Problem," *International Symposium on Formation Flying Missions and Technologies*, CNES, Oct. 2002.

[28] Schaub, H., "Relative Orbit Geometry Through Classical Orbit Element Differences," *Journal of Guidance, Control, and Dynamics*, Vol. 27, No. 5, Sept.–Oct. 2004, pp. 839–848. doi:10.2514/1.12595

[29] Sengupta, P., and Vadali, S. R., "Relative Motion and the Geometry of Formations in Keplerian Elliptic Orbits," *Journal of Guidance, Control, and Dynamics*, Vol. 30, No. 4, July–Aug. 2007, pp. 953–964. doi:10.2514/1.25941

[30] D'Amico, S., and Montenbruck, O., "Proximity Operations of Formation-Flying Spacecraft Using an Eccentricity/Inclination Vector Separation," *Journal of Guidance, Control, and Dynamics*, Vol. 29, No. 3, May–June 2006, pp. 554–563. doi:10.2514/1.15114

[31] Gill, E., D'Amico, S., and Montenbruck, O., "Autonomous Formation Flying for the PRISMA Mission," *Journal of Spacecraft and Rockets*, Vol. 44, No. 3, May–June 2007, pp. 671–681. doi:10.2514/1.23015

[32] Montenbruck, O., Kahle, R., D'Amico, S., and Ardaens, J.-S., "Navigation and Control of the TanDEM-X Formation," *Journal of Astronautical Sciences*, Vol. 56, No. 3, July–Sept. 2008, pp. 341–357. doi:10.1007/BF03256557

[33] D'Amico, S., Ardaens, J.-S., Gaias, G., Benninghoff, H., Schlepp, B., and Jørgensen, J. L., "Noncooperative Rendezvous Using Angles-Only Optical Navigation: System Design and Flight Results," *Journal of Guidance, Control, and Dynamics*, Vol. 36, No. 6, Nov.–Dec. 2013, pp. 1576–1595. doi:10.2514/1.59236

[34] Gim, D.-W., and Alfriend, K. T., "State Transition Matrix of Relative Motion for the Perturbed Noncircular Reference Orbit," *Journal of Guidance, Control, and Dynamics*, Vol. 26, No. 6, Nov.–Dec. 2003, pp. 956–971. doi:10.2514/2.6924

[35] Battin, R. H., *Introduction to the Mathematics and Methods of Astrodynamics*, AIAA, Reston, VA, 1999, pp. 471–514.

[36] Schaub, H., Vadali, S. R., Junkins, J. L., and Alfriend, K. T., "Spacecraft Formation Flying Control Using Mean Orbit Elements," *Journal of Astronautical Sciences*, Vol. 48, No. 1, Jan.–March 2000, pp. 69–87.

[37] Schaub, H., and Alfriend, K. T., "Impulsive Feedback Control to Establish Specific Mean Orbit Elements of Spacecraft Formations," *Journal of Guidance, Control, and Dynamics*, Vol. 24, No. 4, July–Aug. 2001, pp. 739–745. doi:10.2514/2.4774

[38] Hamel, J.-F., and de Lafontaine, J., "Linearized Dynamics of Formation Flying Spacecraft on a J_2-Perturbed Elliptical Orbit," *Journal of Guidance, Control, and Dynamics*, Vol. 30, No. 6, Nov.–Dec. 2007, pp. 1649–1658. doi:10.2514/1.29438

[39] Hamel, J.-F., and de Lafontaine, J., "Neighboring Optimum Feedback Control Law for Earth-Orbiting Formation-Flying Spacecraft," *Journal of Guidance, Control, and Dynamics*, Vol. 32, No. 1, Jan.–Feb. 2009, pp. 290–299. doi:10.2514/1.32778

[40] Alfriend, K. T., Schaub, H., and Gim, D.-W., "Gravitational Perturbations, Nonlinearity and Circular Orbit Assumption Effects on Formation Flying Control Strategies," *Advances in the Astronautical Sciences*, Vol. 104, 2000, pp. 139–158; also *Proceedings of the AAS Guidance, Navigation, and Control Conference*, American Astronautical Soc. Paper 00-012, Feb. 2000.

[41] Brouwer, D., "Solution of the Problem of Artificial Satellite Theory Without Drag," *Astronomical Journal*, Vol. 64, No. 1274, Nov. 1959, pp. 378–397. doi:10.1086/107958

[42] Schaub, H., and Junkins, J. L., *Analytical Mechanics of Space Systems*, AIAA Education Series, 3rd ed., AIAA, Reston, VA, 2014, pp. 811–814.

[43] Alfriend, K. T., and Yan, H., "Evaluation and Comparison of Relative Motion Theories," *Journal of Guidance, Control, and Dynamics*, Vol. 28, No. 2, March–April 2005, pp. 254–261. doi:10.2514/1.6691

[44] Tschauner, J., and Hempel, P., "Rendezvous zu einem in elliptischer Bahn umlaufenden Ziel," *Astronautica Acta*, Vol. 11, No. 5, 1965, pp. 312–321.

[45] Hill, G. W., "Researches in the Lunar Theory," *American Journal of Mathematics*, Vol. 1, No. 1, 1878, pp. 5–26. doi:10.2307/2369430

[46] Clohessy, W. H., and Wiltshire, R. S., "Terminal Guidance System for Satellite Rendezvous," *Journal of the Aerospace Sciences*, Vol. 27, No. 9, 1960, pp. 653–658. doi:10.2514/8.8704

[47] McAdoo, S. F., Jr., Jezewski, D. J., and Dawkins, G. S., "Development of a Method for Optimal Maneuver Analysis of Complex Space Missions," NASA TN-D-7882, April 1975.
[48] Jezewski, D. J., "Primer Vector Theory and Applications," NASA TR-R-454, Nov. 1975.
[49] Lewis, F. L., and Syrmos, V. L., *Optimal Control*, 2nd ed., Wiley, New York, 1995, pp. 41–66, 281–311.
[50] Lion, P. M., and Handelsman, M., "Primer Vector on Fixed-Time Impulsive Trajectories," *AIAA Journal*, Vol. 6, No. 1, Jan. 1968, pp. 127–132.
[51] Jezewski, D. J., and Rozendaal, H. L., "Efficient Method for Calculating Optimal Free-Space N-Impulse Trajectories," *AIAA Journal*, Vol. 6, No. 11, Nov. 1968, pp. 2160–2165. doi:10.2514/3.4949
[52] Antsaklis, P. J., and Michel, A. N., *A Linear Systems Primer*, Birkhäuser, New York, 2007, pp. 487–497.
[53] Neustadt, L. W., "Optimization, a Moment Problem, and Nonlinear Programming," *SIAM Journal on Control and Optimization*, Vol. 2, No. 1, 1964, pp. 33–53. doi:10.1137/0302004
[54] Potter, J. E., and Stern, R. G., "Optimization of Midcourse Velocity Corrections," *Proceedings of the IFAC Symposium on Automatic Control in the Peaceful Uses of Space*, edited by Aseltine, J. A., Plenum, New York, June 1965, pp. 70–84.